TERRAIN MAPPING AND POSE ESTIMATION FOR POLAR SHADOWED REGIONS OF THE MOON

Virtual Conference 19-23 October 2020

Haidar Jamal, Vaibhav Gupta, Neil Khera, Srinivasan Vijayarangan, David S. Wettergreen, William L. (Red) Whittaker

The Robotics Institute, Carnegie Mellon University, Pittsburgh, PA, USA, Email: hjamal@andrew.cmu.edu

ABSTRACT

Lunar ice, likely to be found in the highest abundance near the poles, could be a source of water for drinking, oxygen for breathing, and for producing propellants for venturing beyond the moon to deep space. Viability depends on specifics of the accessibility, depth, and concentration of the ice, which can only be determined by surface missions of repeated robotic explorations over time. Remote sensing indicates that ice concentrates in low, shadowed depressions that may or may not be close to safe landing sites [1]. Navigating through polar shadows and darkness necessitates capability for sensing in the dark. This paper profiles the perception system of MoonRanger, a micro-rover manifested on a 2022 NASA CLPS flight [2], which will be the first polar mission to perform *in situ* measurement of lunar ice.
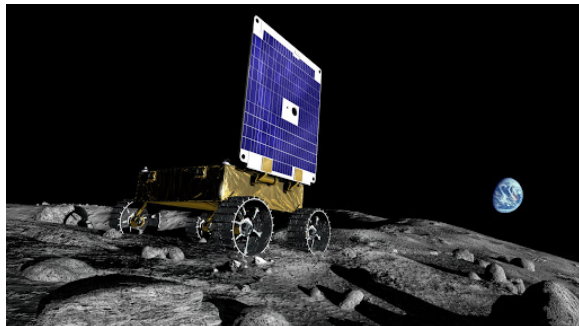
Figure 1: Artist rendering of MoonRanger

1 INTRODUCTION

This paper addresses the challenges of and solutions for micro-rover perception in darkness, navigation and mapping autonomy with limited computing and energy. We propose a computationally-inexpensive and low-power localization and mapping solution for rover navigation in darkness through projection of light stripes, monocular vision, wheel encoding, and inertial sensing. Our approach extends the work done in [3] by requiring one camera instead of two, using multiple lasers, providing a calibration scheme for the lasers, and a complete localization and mapping solution.

Before runtime, we use a camera-calibration grid to calibrate the lasers through the process outlined by [4].

As the rover drives, the vision system captures images of the laser-lines on the approaching terrain. The calibration enables the generation of 3D scan lines in the rover's local reference frame. We fuse these scan-lines into a global point cloud using a pose estimate from an Extended Kalman Filter [5] that uses wheel encoding and inertial measurement data.

This paper is organized as follows. In section 2, we describe the light striping technique for 3D reconstruction. In section 3, we derive the calibration of the light stripe system. In section 4, we describe the Extended Kalman Filter used aboard MoonRanger for pose estimation. In section 5, we combine the pose estimates with the light stripe to generate the point cloud used for terrain mapping. We analyze the integrated perception system on test data in a laboratory setting and discuss the viability of the system for the MoonRanger mission.

2 LIGHT STRIPING RECONSTRUCTION

Key to any robotic mapping solution is the measurement of the position of points on the terrain surface. Environmental conditions and application specific requirements dictate the use of particular algorithms and sensors. A large class of sensors are impossible for MoonRanger given the extreme environment of space, the rover's power budget, and the mission's financial budget for hardware. Furthermore, the rover's on board computer is responsible for running numerous processes simultaneously, including communication, planning, and health monitoring, severely limiting the available resources.

With its limited computing, the Mars Sojourner rover employed a simple but robust system using multiple light stripes and a pair of cameras [6]. The onboard algorithm analyzed deviations in the stripes to determine if an obstacle lay ahead. Depending on the image, it would navigate in one of a set of fixed motion sequences. This system was suitable due to the low computational overhead and the availability of space-worthy cameras and lasers.

Inspired by the success of this system and accounting for our mission constraints, we will use a light stripe

based mapping algorithm aboard MoonRanger. Our algorithm processes images of the lasers to generate a 3D point cloud model of the terrain. Reconstruction using light stripes has been known since the 1970s [7] [8] [9] and has proven successful in many application areas.

Our reconstruction algorithm requires a monocular camera and at least one planar light stripe fixed relative to each other. Multiple light stripes increase the density of the constructed map and allow for detection at different distances at the cost of increased computational overhead, power consumption, and mass. After testing numerous configurations, we opted for two horizontal light stripes for MoonRanger, shown in Fig. 2.
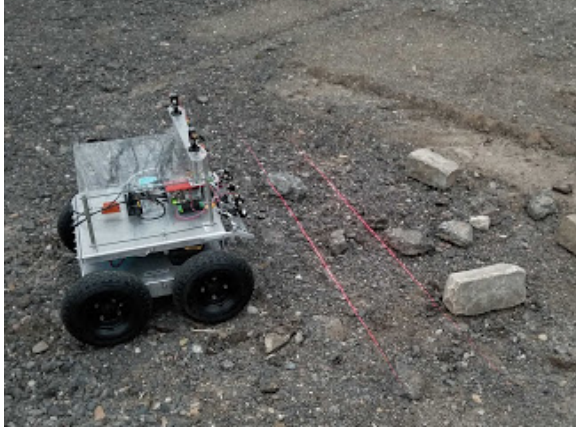

Figure 2: Dual-laser setup on a testing platform

The first step of setting up the algorithm is to calibrate the camera for its calibration matrix [10]

$$K = \begin{bmatrix} f_x & 0 & c_x \\ 0 & f_y & c_y \\ 0 & 0 & 1 \end{bmatrix}, \qquad (1)$$

where f_x and f_y are the focal lengths of the sensor x and y dimensions and (c_x, c_y) is the optical center of the camera in pixels and its distortion parameters and its the radial distortion coefficients, k_1, k_2, and k_3, and tangential distortion coefficients, p_1 and p_2.

We then determine the plane equation of the light stripe relative to the camera as shown in Fig. 3.

$$AX + BY + CZ + D = 0 \qquad (2)$$

The procedure to determine this plane follows the methodology of [4] and is described in detail in section 3.

With this plane equation, a pixel (x,y) is mapped to the 3D coordinates (X, Y, Z) with the following equations [10]:
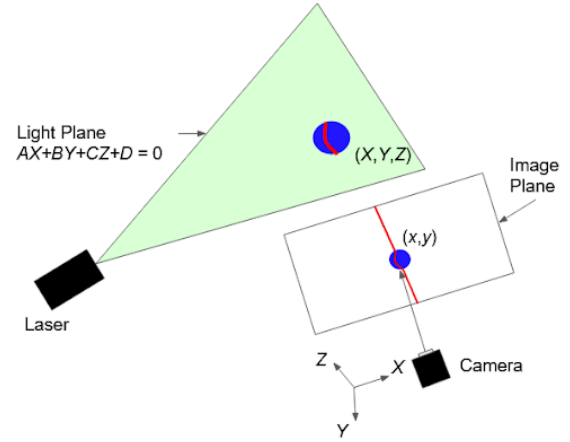
$$X = \frac{x - c_x}{f_x} Z \qquad (3)$$

Figure 3: Light plane relative to camera

$$Y = \frac{y - c_y}{f_y} Z \qquad (4)$$

$$Z = \frac{-D f_x f_y}{A(x - c_x)f_y + B(y - c_y)f_x + C f_x f_y} \qquad (5)$$

A typical view from the onboard camera of the rover is shown in Fig. 4. With classical image processing techniques [11], the pixel coordinates of the laser in the image is found and then mapped to 3D points using Eqs. 3-5. Each image outputs a set of 3D points in the camera's coordinate frame. The frequency of images is increased at the cost of greater computational overhead. Since MoonRanger travels at its fastest speed at 5 cm/s, a processing time of 2 Hz is sufficient for a high quality reconstruction.

To fuse the 3D points taken in a sequence of images into the global frame, the camera's transform in the global frame for each image is necessary. This transform can be determined with a pose estimation algorithm paired with knowledge of the fixed configuration of the camera relative to the pose estimation coordinate frame.

3 LIGHT STRIPING CALIBRATION

The plane of the light stripe relative to the camera is found through computing multiple 3D points along the stripe and fitting a plane through these points. Calibration techniques differ in the manner in which these 3D points are found. Following the methodology of [4], we use a planar checkerboard pattern to compute these points. This technique is very similar to calibrating a camera using Zhang's method [12], and the same checkerboard calibration pattern can be used for both procedures. We present our implementation of [4]
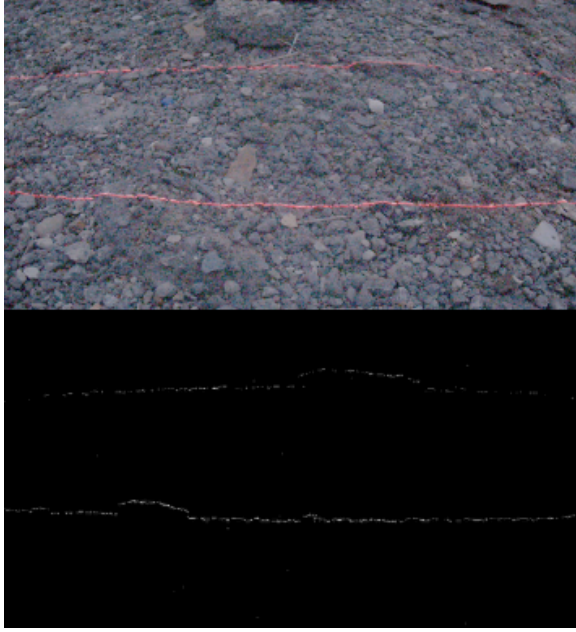
Figure 4: Above: Light Stripe in Rocky Terrain. Below: Laser pixel coordinates found through image processing

along with additions, and refer the reader to the original paper for a detailed derivation. Our software for calibration has been made open source and is available at [26].

After having calibrated the camera for its intrinsic parameters, we generate a sequence of images of the light stripe projected onto the checkerboard calibration pattern, such as in Fig. 5.
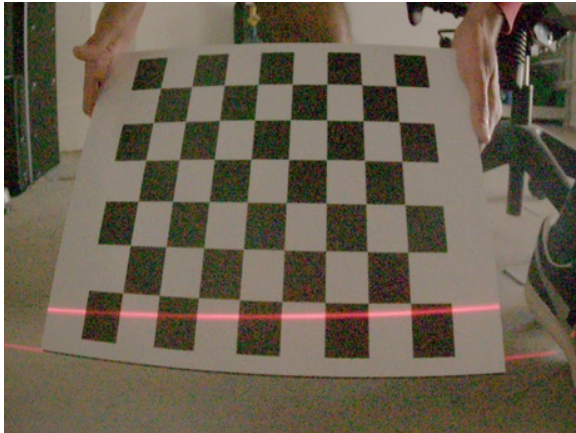

Figure 5: Light Stripe Projected on Checkerboard Calibration Pattern

For each image, we use the calibration matrix and distortion parameters to undistort the image. In 3D space the laser intersects the calibration grid at some Q between some three known points A, B, and C, as shown

in Fig. 6. In the image plane, these points correspond to 2D coordinates q, a, b, and c.
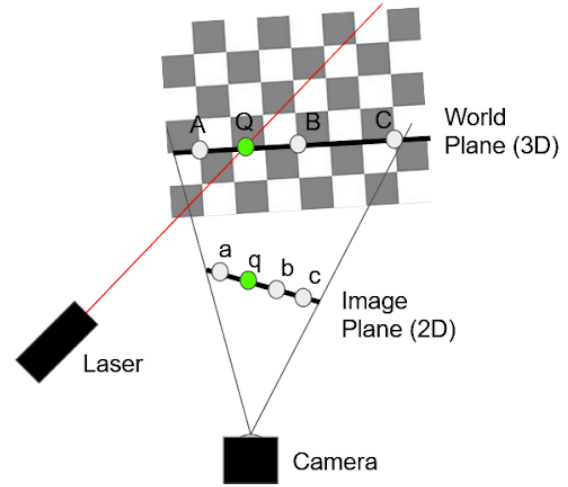

Figure 6: Both sets of points in 3D and 2D

The geometric property of the cross ratio is preserved between the two line segments containing the points [4][13]:

$$CR(a, q, b, c) = CR(A, Q, B, C) \tag{6}$$

where

$$CR(A, B, C, D) = \frac{\overline{AC}}{\overline{BC}} \frac{\overline{BD}}{\overline{AD}} \tag{7}$$

and $\overline{xy}$ is the Euclidean distance between points x and y, either in 2D or 3D.

Since the dimensions of the squares of the checkerboard are known, we can fix a world frame to the upper left corner of the checkerboard and determine A, B, and C. To find a, b, and c, we use the Harris corner detector typically found in camera calibration packages [14] to determine their pixel coordinates in the image frame. We convert them to the normalized camera frame by applying K^{-1} to extract coordinates a, b, and c. To find point q, we use image processing techniques to find the intersection between the light stripe and the line segment $\overline{ac}$, as shown in Fig. 7.

Substituting all of the values in Eq. 7 and another constraint $\overline{QB} + \overline{BC} = \overline{QC}$, we can solve for $\overline{QB}$ and $\overline{QC}$ and then extract Q. Since Q is in the world frame of the checkerboard calibration pattern, we need to transform it to the camera frame.

We use Perspective-n-Point algorithm [14][15] on the original image to find the transformation from the world frame to the camera frame, and use this transformation to find Q_c, the point Q in the camera frame.
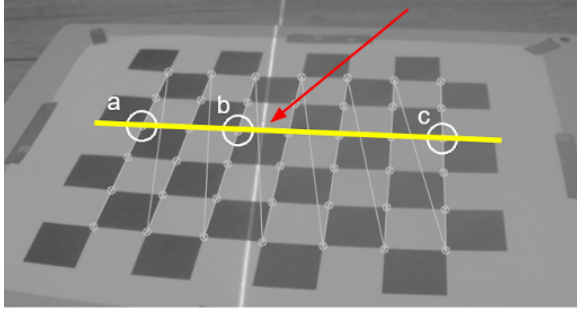
Figure 7: Search for point q between points a and c in the image

We repeat the procedure to obtain at least three non-collinear points on the laser plane. Then we solve for the plane equation (Eq. 2) using the RANdom SAmple Consensus (RANSAC) algorithm [16] and singular value decomposition [17].

4   POSE ESTIMATION

Navigation in shadowed regions prevents the use of the visual odometry techniques used for modern space rovers [18]. In these dark regions, MoonRanger will have to rely on its inertial measurement unit (IMU) and wheel encoding for pose estimation. For the mission, we selected the STIM-300 from Sensonor [19]. This device has undergone extensive environmental testing for space qualification and flown on previous CubeSat missions.

To fuse together the IMU and wheel encoding data, an Error-State Extended Kalman Filter was developed based on [3] and [20]. Similar systems have proven highly successful for commercial and research applications [21] [22]. The details of the derivation of the algorithm can be found with its open source implementation at [25].
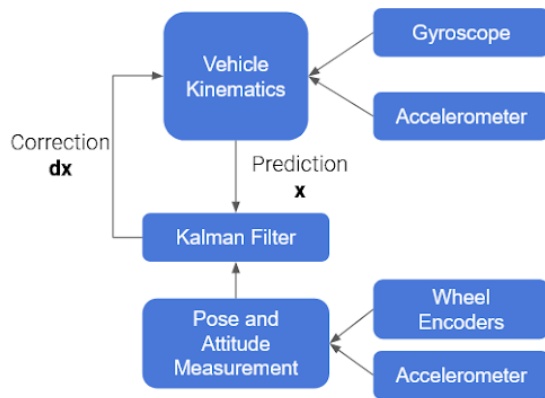

Figure 8: Kalman Filter Block Diagram

A block diagram of the subsystem is shown in Fig. 8. In our algorithm, we estimate the position, velocity, orientation, gyroscope bias, and accelerometer bias. The accelerometer and gyroscope are integrated to predict position, and this prediction is periodically corrected using a kinematic model of the rover fed data from wheel encoders. While the rover is stationary, the accelerometer is used to correct orientation [3]. The implementation can easily be modified for regions where additional sensors can be used such as sun sensors for heading correction and visual odometry for pose and attitude correction.

One key difference between this algorithm running on Earth and on the Moon is the value of the gravitational constant. With a rough knowledge of the landing site, this value can be predetermined using existing gravity field models of the lunar surface [23]. Furthermore, many algorithms take into account the rotation of the Earth for higher fidelity models of the dynamics. These terms were neglected in our derivation.

5   INTEGRATED PERCEPTION PIPELINE

With the combination of light stripe calibration, reconstruction, and a version of the pose estimation algorithm, the proposed solution was tested in a laboratory setting, as shown in Fig. 9. The rover was manually driven straight on a smooth floor through a set of obstacles in a dark room, taking images at 2 Hz. Although five lasers can be observed in the figure, only the two red horizontal lasers were used in the algorithm. All lasers were calibrated following the methodology in section 3. Fusing the reconstruction of 3D data for each image from section 2 and integrating only wheel encoder data, a point cloud was generated as shown in Fig. 10. In the figure, varying color demonstrates the change in elevation.

Although this result gives a geometrically accurate and dense reconstruction of the terrain for a benign laboratory setting, the system's capability for reconstruction in outdoor rough terrain remains to be determined. The quality of the reconstructed map depends significantly on the quality of pose estimation. In an outdoor setting, the rover would be susceptible to slip, falling over rocks, and driving over rising or descending terrain, all of which would drastically influence the quality of the pose estimate and hence the output of the map.

Nonetheless, we can conclude that given a high quality pose estimate, the light striping technique is capable of generating a dense and appropriately scaled pointcloud usable in obstacle avoidance and mapping algorithms such as [24]. Further outdoor testing with the filter developed in section 4 will be performed to quantify
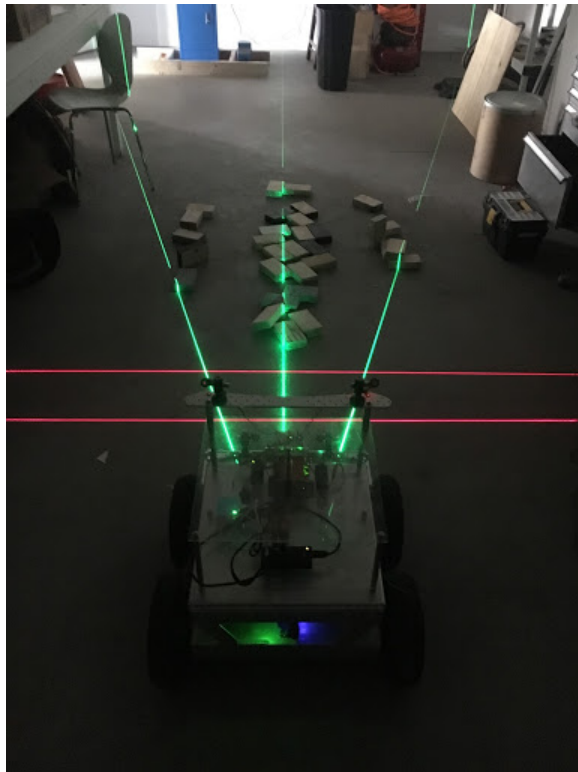
Figure 9: Integrated Light Striping Reconstruction and Pose Estimator

the capability of the overall system.

6 CONCLUSION

The core result is that our method can provide an accurately scaled and dense point cloud in a completely dark setting, given a reasonable pose estimate. We provide an easy method to set up the system by calibrating light stripes using a checkerboard pattern and using them as part of a reconstruction algorithm.

In its current form, the calibration for the camera and light striping system would be prepared pre-flight. This is a risk to the mission since the launch could slightly displace parts and the space environment could affect the material properties of the camera sensor. In future work we will investigate the extension of the algorithm for live calibration as well as quantify the changes in calibration for a variety of environmental conditions. The orientation and number of lasers will also be selected. The system will then be formally engineered to meet launch standards. The algorithm will need to be tested in rough terrain where the pose estimation algorithm performance will likely deteriorate. Given the algorithm can pass the above tests, we feel that the system provides a low cost, low power, and high quality map that MoonRanger can use to drive safely in the shadowed regions of the Moon.
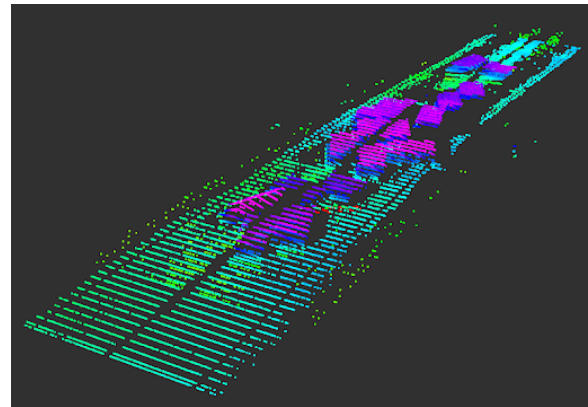

Figure 10: Integrated Light Striping Reconstruction and Pose Estimator

References

[1] Li, S., Lucey, P. G., Milliken, R. E., Hayne, P. O., Fisher, E., Williams, J. P., ... & Elphic, R. C. (2018). Direct evidence of surface exposed water ice in the lunar polar regions. Proceedings of the National Academy of Sciences, 115(36), 8907-8912.

[2] NASA. Available at: https://www.nasa.gov/press-release/nasa-awards-contract-to-deliver-science-tech-to-moon-ahead-of-human-missions

[3] Pedersen, L., Han, C. S., & Vitus, M. (2008, February). Dark navigation: Sensing and rover navigation in permanently shadowed lunar craters. In International Symposium on Artificial Intelligence, Robotics and Automation in Space (i-SAIRAS), Los Angeles, CA.

[4] Zhou, F., & Zhang, G. (2005). Complete calibration of a structured light stripe vision sensor through planar target of unknown orientations. Image and Vision Computing, 23(1), 59-67

[5] Farrell, J. (2008). Aided navigation: GPS with high rate sensors. McGraw-Hill, Inc..

[6] Schenker, P., Sword, L., Ganino, A., Bickler, D., Hickey, G., Brown, D., ... & Aghazarian, H. (1999). Lightweight rovers for Mars science exploration and sample return.

[7] Jalkio, J. A., Kim, R. C., & Case, S. K. (1985). Three dimensional inspection using multistripe structured light. Optical Engineering, 24(6), 246966.

[8] Levoy, M., Pulli, K., Curless, B., Rusinkiewicz,

S., Koller, D., Pereira, L., ... & Shade, J. (2000, July). The digital Michelangelo project: 3D scanning of large statues. In Proceedings of the 27th annual conference on Computer graphics and interactive techniques (pp. 131-144).

[9] Simon, D. A., Hebert, M., & Kanade, T. (1994, May). Real-time 3-D pose estimation using a high-speed range sensor. In Proceedings of the 1994 IEEE International Conference on Robotics and Automation (pp. 2235-2241). IEEE.

[10] Szeliski, R. (2010). Computer vision: algorithms and applications. Springer Science & Business Media.

[11] Zhang, T. Y., & Suen, C. Y. (1984). A fast parallel algorithm for thinning digital patterns. Communications of the ACM, 27(3), 236-239.

[12] Zhang, Z. (2000). A flexible new technique for camera calibration. IEEE Transactions on pattern analysis and machine intelligence, 22(11), 1330-1334

[13] Brannan, D., Esplen, M., & Gray, J. (1999). Geometry. Cambridge: Cambridge University Press. doi:10.1017/CBO9780511807503

[14] Bradski, G., & Kaehler, A. (2008). Learning OpenCV: Computer vision with the OpenCV library. " O'Reilly Media, Inc.".

[15] Lepetit, V., Moreno-Noguer, F., & Fua, P. (2009). Epnp: An accurate o(n) solution to the pnp problem. International journal of computer vision, 81(2), 155.

[16] Fischler, M. A., & Bolles, R. C. (1981). Random sample consensus: a paradigm for model fitting with applications to image analysis and automated cartography. Communications of the ACM, 24(6), 381-395.

[17] Shlens, J. (2014). A tutorial on principal component analysis. arXiv preprint arXiv:1404.1100.

[18] Maimone, M., Cheng, Y., & Matthies, L. (2007). Two years of visual odometry on the mars exploration rovers. Journal of Field Robotics, 24(3), 169-186.

[19] Sensonor. STIM 300. Available at: https://www.sensonor.com/products/inertial-measurement-units/stim300/

[20] Crassidis, J. L. (2006). Sigma-point Kalman filtering for integrated GPS and inertial navigation. IEEE Transactions on Aerospace and Electronic Systems, 42(2), 750-756.

[21] Moore, T., & Stouch, D. (2016). A generalized extended kalman filter implementation for the robot operating system. In Intelligent autonomous systems 13 (pp. 335-348). Springer, Cham.

[22] Yi, J., Zhang, J., Song, D., & Jayasuriya, S. (2007, October). IMU-based localization and slip estimation for skid-steered mobile robots. In 2007 IEEE/RSJ International Conference on Intelligent Robots and Systems (pp. 2845-2850). IEEE.

[23] Hirt, C., & Featherstone, W. E. (2012). A 1.5 km-resolution gravity field model of the Moon. Earth and Planetary Science Letters, 329, 22-30.

[24] Wettergreen D., & Wagner M. (2012) i-SAIRAS "Developing a framework for reliable autonomous surface mobility"

[25] Haidar Jamal. (2020). hjamal3/encoder_imu_ekf_ros: First release of algorithm (Version v1.0). Zenodo. http://doi.org/10.5281/zenodo.4033638

[26] Haidar Jamal. (2020). hjamal3/Light-Stripe-Calibration (Version v1.0). Zenodo. http://doi.org/10.5281/zenodo.4036771